NANO LETTERS

2008
Vol. 8, No. 8
2321-2327

A Hybrid Plasmonic−Photonic Nanodevice for Label-Free Detection of a Few Molecules

Francesco De Angelis,[†,‡] Maddalena Patrini,[§] Gobind Das,[†,‡] Ivan Maksymov,[§] Matteo Galli,[§] Luca Businaro,[||] Lucio Claudio Andreani,[§] and Enzo Di Fabrizio*[,†,‡,||]

BIONEM laboratory, University of Magna Graecia, Campus S. Venuta, Germaneto, viale Europa, 88100 Catanzaro, Italy, CNISM and Department of Physics "A. Volta", University of Pavia, via Bassi 6, 27100 Pavia, Italy, TASC National Laboratory, CNR-INFM, Area Science Park, Basovizza, 34012 Trieste, Italy, and CalMED s.r.l., Campus S. Venuta, Germaneto, viale Europa, 88100 Catanzaro, Italy

Received April 18, 2008; Revised Manuscript Received June 6, 2008

ABSTRACT

Noble metal nanowaveguides supporting plasmon polariton modes are able to localize the optical fields at nanometer level for high sensitivity biochemical sensing devices. Here we report on the design and fabrication of a novel photonic−plasmonic device which demonstrates label-free detection capabilities on single inorganic nanoparticles and on monolayers of organic compounds. In any case, we determine the Raman scattering signal enhancement and the device detection limits that reach a number of molecules between 10 and 250. The device can be straightforwardly integrated in a scanning probe apparatus with the possibility to match topographic and label-free spectroscopic information in a wide range of geometries.

The interest in knowing the spectroscopic signature of a single molecule is wide and spans from physics, chemistry, and material science to biology, where DNA or protein mutation due to a single gene or amino acid can be evidenced.[1] From an optical point of view, the detectability of a few molecules is related to the spatial confinement of the electromagnetic field. The interest here is not only in the detection of isolated molecules placed at specific "hot spots" but also in employing dense samples where the molecules are in proximal contact. Strong progress has been done in the past decade in breaking the Abbe diffraction limit by developing new approaches in fluorescence spectroscopy.[2,3] Further progress in the knowledge of the status of a few molecules can be done if the detection is accomplished by Raman scattering spectroscopy.[4−6] In fact, being based on a second-order optical response, Raman spectroscopy is not affected by photobleaching, and molecule photodamage is strongly reduced as compared to first-order spectroscopy. In the last 5 years, there has been a burst in the study and conceiving of new devices for the generation of surface plasmon polaritons (SPPs) confined at the nanoscale,[7−10] where radiation−matter interaction is strongly enhanced. Several fabrication methods are now available for material preparation and surface nanostructuring,[11,12] but only a few of them can ensure the stringent design control needed for an efficient and reproducible generation and manipulation of SPPs. Recent advances in optical investigations have been obtained amplifying the local electromagnetic (e.m.) field either by exploiting "hot spot" sites, capable of providing surface enhanced Raman scattering (SERS),[13−15] or adopting subwavelength scatterers such as metallic tips and nanoparticles in near-field configurations (tip-enhanced Raman scattering (TERS) and gap-mode TERS).[16,17] Due to the intrinsic collective nature of SPP excitation,[18] there are several conditions to be satisfied simultaneously for their effective generation.[7] Generally speaking, when local excitation is used for the detection of molecules, the metrological control of elemental surface unit has to reach the nanometer scale. For instance, when nanostructured colloidal or metallic surfaces are used in the case of a nanoantenna, two length scales are relevant: the diameter (d) of the elemental structure and the mutual distance (Δ) between two nanostructures. As a rule of thumb, one should keep $d \sim \lambda/10$ and $\Delta \sim \lambda/100$, where λ is the excitation wavelength used.[19] Such stringent conditions force the choice toward top-down fabrication techniques that guarantee a strict dimensional and geometrical control.

* Corresponding author, difabrizio@tasc.infm.it.
† University of Magna Graecia.
‡ CalMED s.r.l.
§ University of Pavia.
|| TASC National Laboratory, CNR-INFM.

10.1021/nl801112e CCC: $40.75
Published on Web 07/17/2008

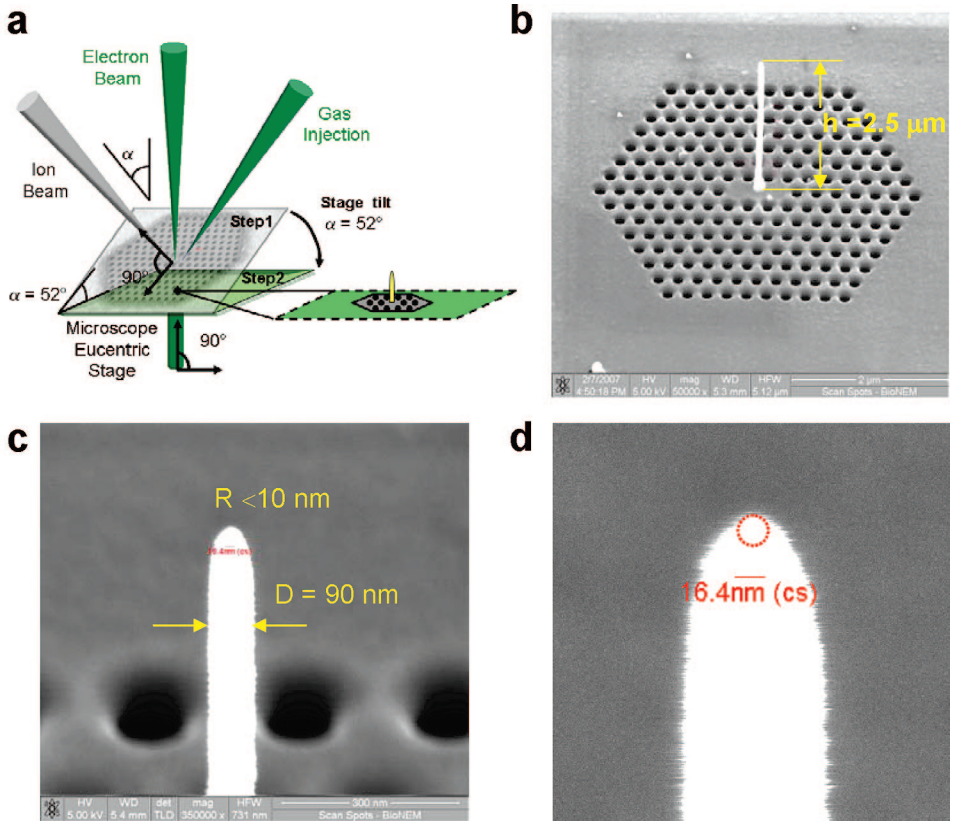

Figure 1. Fabrication setup and SENSe device. (a) Scheme of the dual beam fabrication system based on focused ion milling (step 1) and electron beam induced deposition (step 2) with a gas injection system. (b) SEM image of the whole device including the photonic cavity and, at its center, the plasmonic nanoantenna. The latter is 2.5 μm high, and its size gradually decreases from 90 nm in diameter at bottom down to 10 nm radius of curvature at the tip. (c, d) SEM details of the nanoantenna tip and its radius of curvature.

Here we report on the design and fabrication of a novel nano-optical device for biosensing, and we demonstrate its detection capabilities on SiO_x nanoparticles, on a single CdSe quantum dot, and on a monolayer of organic compounds. In all cases, the number of molecules involved covers a range between 10 and 200. The detection is accomplished by far field Raman scattering spectroscopy operating in the sub-diffraction regime. The working principle combines the light harvesting capabilities of a dielectric photonic crystal cavity with the extraordinary confining properties of a metallic nanowaveguide. This leads to efficient optical excitation of target samples through surface plasmon polariton modes localized at nanoscale, as demonstrated by Raman scattering measurements, in confocal configuration, and confirmed by numerical calculations. The present results, demonstrating label-free detection of a few molecules in subwavelength regime and in far field configuration, open up new perspectives toward single-molecule detection. Our nanolithography techniques of choice in this work rely on two powerful fabrication methods: focused ion beam (FIB) milling[20] and chemical vapor deposition (CVD) induced by a focused electron beam. The device consists of a plasmonic nanoantenna with an ogival-shaped tip made of a nobel metal, such as gold or silver, combined with a photonic crystal (PC) cavity. The fabrication technique and the scanning electron microscope image of a SENSe (surface-enhanced nanosensor) device are shown in Figure 1. The PC cavity produces an efficient coupling between the external optical source and the nanoantenna (direct coupling of the far field to the nanoantenna in the absence of a PC is inefficient, as we observed both theoretically and experimentally). The nanoantenna placed at the PC cavity center supports SPP modes and acts as a nanoscale waveguide, able to propagate and focus the SPP toward the tip where strong enhancement of the e.m. field intensity occurs. In this work detection of a few molecules localized at the nanometer scale of the tip, in label-free conditions, is experimentally demonstrated by Raman scattering measurements in the far field.

The geometry of the metallic nanoantenna plays an important role in defining the SPP mode profile details. When the nanoantenna shape is perfectly conical, an adiabatic behavior is predicted.[21,22] This causes the SPP field to be effective for scattering emission only at the tip where an enhancement factor of about 10^3 for the electrical field is theoretically reachable.[23] In our case the nanoantenna has an ogival shape, which is easier to fabricate without failing in device performance. In fact, both our theoretical simulations and Raman scattering experiments confirm that the SPP mode is strongly localized in a region comparable to the radius of curvature of the tip (about 10 nm), providing efficient coupling for scattering events in the far field.

As the ultimate task, the device is conceived to detect a few molecules in a far field configuration through Raman scattering spectroscopy. We aim at achieving unambiguous chemical information of molecular species localized in a region down to 10 nm and in label-free conditions. The major

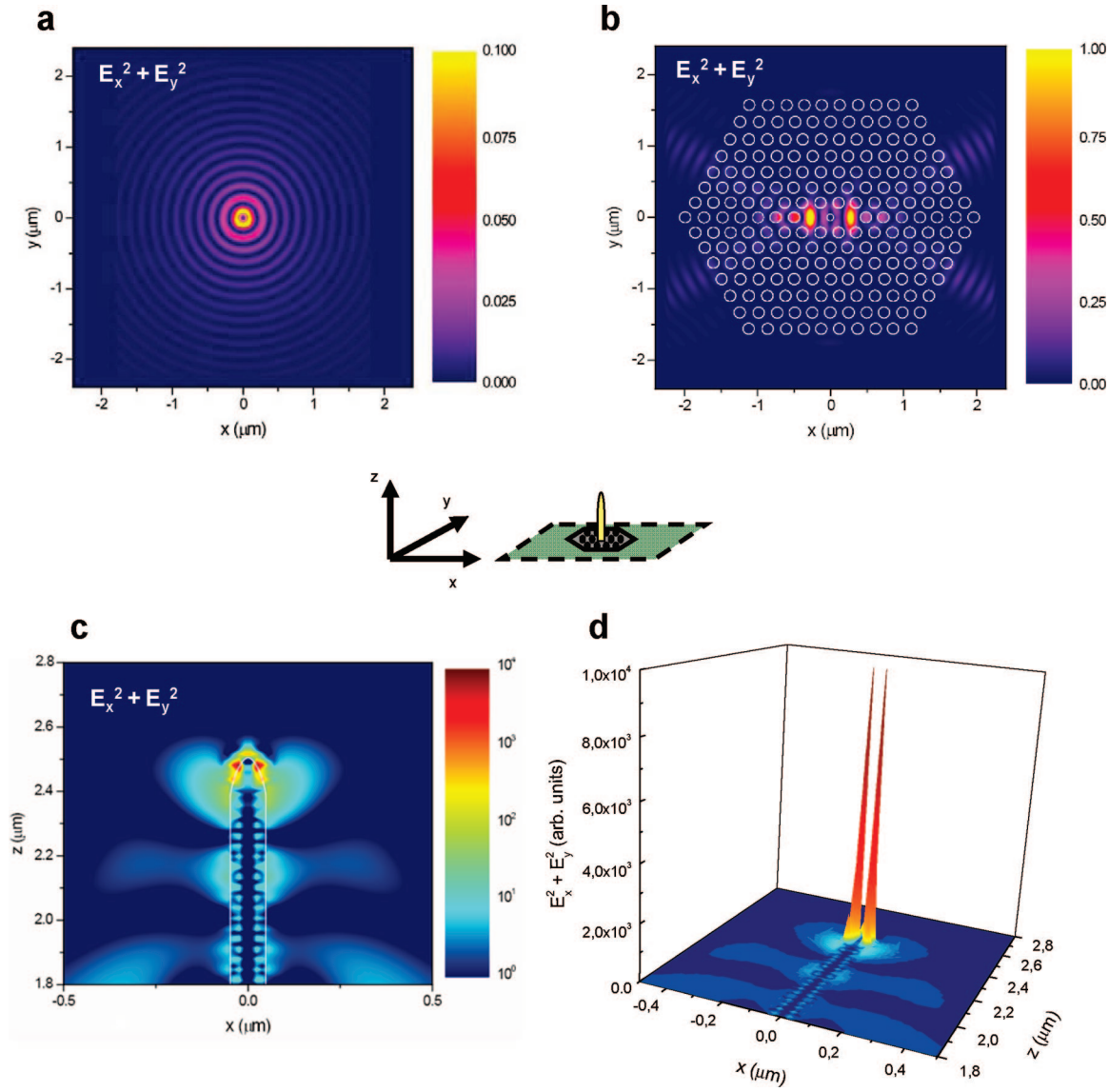

Figure 2. FDTD calculation of nanoantenna optical response. The adopted reference system *x*,*y*,*z* is sketched for clarity. Color scales of panels a−d are in arbitrary units. The numerical values reported in the color scale are in the correct relative intensity values. (a) Spatial $E_x^2 + E_y^2$ field profile of the plasmonic nanoantenna on a silicon nitride membrane calculated at $\lambda = 514$ nm. (b) Spatial $E_x^2 + E_y^2$ field profile of the overall device calculated at $\lambda = 514$ nm. (c) Spatial $E_x^2 + E_y^2$ field profile propagating along nanoantenna calculated at $\lambda = 514$ nm. (d) 3D profile of $E_x^2 + E_y^2$ field intensity along the nanoantenna. The SPP mode is strictly confined at the tip. In our 3D profile, we can simulate a minimum radius curvature of 20 nm. The distance between the two intensity peaks is related to the minimum cell size (see Supporting Information) adopted in the FDTD calculation and results to be twice the radius of curvature. The overall electrical field enhancement at the tip is 100.

advantages of the present device are that the nanoantenna provides a considerable SPP enhancement and that the excitation source (focused on the PC cavity) is spatially separated from the Raman active site. This decreases the perturbation effects of the source and the background signal and provides increased sensitivity down to detection of a few molecules. For the above reasons, the present experimental configuration is distinguished from the current research efforts in few molecule detection based on tip-enhanced near-field configurations (SERS, TERS, gap-mode TERS) where excitation and detection sites are spatially coincident.

The device fabrication starts defining, by a FIB milling process, the photonic cavity (PC) that consists of a very high quality Si_3N_4 membrane[24] (100 nm thick, dielectric constant $\epsilon = 4$ in the visible range) with a triangular lattice of air holes. The lattice constant a is 250 nm, and the hole radius r is $0.3a$. A L3-type PC cavity is formed by three missing holes at the center of the patterned area and along the Γ−K direction. In a second step the platinum nanoantenna is deposited at the cavity center exploiting chemical vapor deposition (CVD) induced by a focused electron beam (Figure 1a) from a gas precursor of $(CH_3)_3Pt(C_pCH_3)$. After the growth of the nanoantenna, a thin film of gold (30 nm thick) has been deposited on the sample and removed from the PC (but not from the nanoantenna) using FIB milling. A scanning electron microscope (SEM) image of the overall device is shown in Figure 1b, with a blow up of the nanoantenna tip in panels c and d of Figure 1 (see Supporting Information section 1).

The PC structure containing a L3-type cavity is designed[25,26] by a guided-mode expansion method in order to have a cavity mode in the green spectral region. Its spectral response (Supporting Information section 2) is simulated by using both guided-mode expansion method and finite-difference time domain (FDTD) code.[27,28] When the nanoantenna is absent, we observe a strong peak at 2.31 eV corresponding to the fundamental TE cavity mode. However, when the nanoantenna is added, the peak is strongly suppressed indicating that the energy of the PC cavity mode is converted in the SPP mode of the nanoantenna. The square module of the e.m. field ($E^2 = E_x^2 + E_y^2$) in the membrane plane is calculated in the presence of the nanoantenna, without (Figure 2a) and with (Figure 2b) the photonic crystal cavity, by comparison of the two panels, the energy-concentration action operated by the PC cavity on the nanoantenna is readily apparent (notice the different color scales in the two panels). The intensity ratio, evaluated at the same exciting power, is one order of magnitude in favor of the nanoantenna on the PC cavity.

SPP propagation along the nanoantenna and its strong localization at the tip are evidenced by FDTD simulations: the calculated SPP 2D map in the *xz* plane and 3D plot of E^2 intensity in the nanoantenna are shown in panels c and d of Figure 2, respectively. Due to FDTD minimum cell size (Supporting Information section 2) adopted in the calculation, we simulate a minimum radius curvature of 20 nm. This causes the appearance of two distinct peaks (they are due to a numerical calculation grid that in our case has a minimum lateral size of 13 nm). The distance between the peaks is twice the radius of curvature and it scales down with the radius of curvature; thus it would go to zero with a vanishing mesh size. The simulation allows evaluation of the electrical field enhancement factor (the ratio between the incoming electrical field at the bottom of the nanoantenna and the electrical field at the tip) to be about 100. For an ideal cone geometry the enhancement factor can be higher at the tip;[21] however in the present nanoantenna structure it is limited by the radius of curvature at the apex, which is about 10 nm (see Figure 1). Since we simulate a radius of curvature of 20 nm, our calculated enhancement factor is expected to be close to the one of the actual device.

A direct way to probe our device performance is to design far-field Raman scattering experiments in order to detect the spectroscopic signal from the nanoantenna. According to FDTD modeling, the plasmonic field is localized around the tip with a decaying length comparable to its radius of curvature. In order to experimentally demonstrate this, we fabricated/deposited on the nanoantenna different nanomaterials, acting as local scatterers, with nanometric positioning control. In the experimental scheme a visible laser is the optical external source (Ar^+ laser source at 514 nm) and it is focused on the PC cavity that resonantly excites the SPP mode in the nanoantenna. The experimental setup (see Supporting Information section 3) consists of a commercial micro-Raman system whose excitation/detection optical path is modified for transmission geometry that optimizes sample illumination.

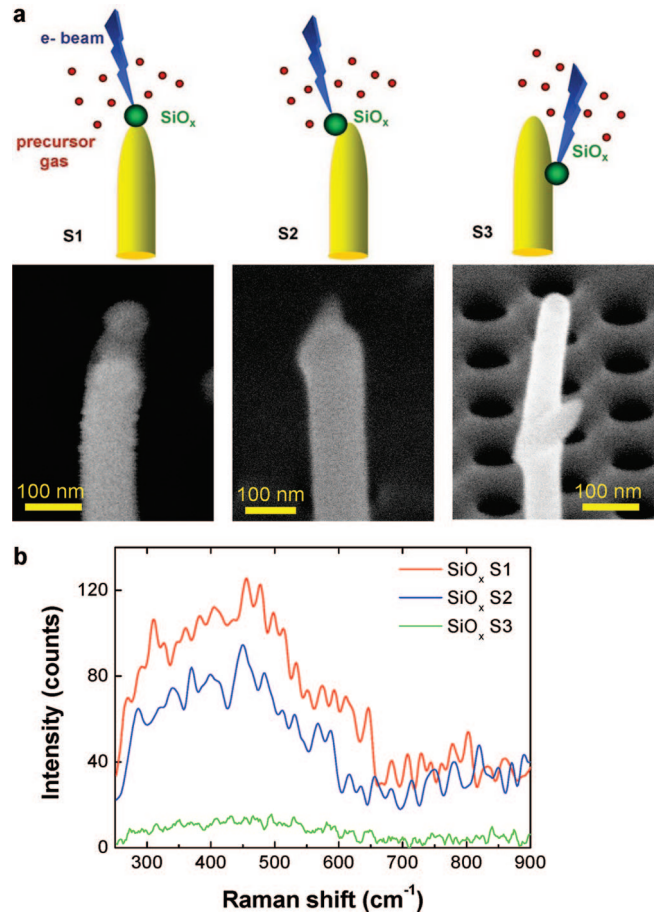

Figure 3. SiO_x deposition on the nanoantenna. (a) Schematic and SEM images of the SiO_x nanoparticle deposition at three different positions on the nanoantenna, named, S1, S2, and S3, corresponding to the tip apex, near the apex, and along the nanoantenna wall, respectively. (b) Raman scattering spectra ($\lambda_{exc} = 514$ nm, $P = 0.18$ mW, $T_{int} = 100$ s) of a SiO_x nanoparticle deposited on the nanoantenna at positions S1, S2, and S3.

First we deposit SiO_x nanoparticles on the nanoantenna with nanometric spatial control by using CVD deposition induced by focused electron beam (see Supporting Information sections 4 and 5). Figure 3a shows the results of e-beam deposition of a SiO_x nanoparticle as a function of three positions along the nanoantenna. The deposition of SiO_x is done by using electron beam induced deposition from the precursor gas TEOS (tetraethylorthosilicate). The SiO_x nanoparticle is selectively deposited in a specific position by focusing and positioning the electron beam, with nanometer precision with the aid of dedicated software. The electron beam is "on" for few seconds in the presence of a stationary flow of precursor gas. SiO_x is deposited, for each sample, at three different positions named S1, S2, and S3.

The corresponding Raman measurements are reported in Figure 3b. The experimental results show that the maximum signal is obtained when the SiO_x nanoparticle is deposited at the tip center (red line) of the nanoantenna and it rapidly vanishes as soon as the particle is deposited away from the tip (blue line). From SEM investigations we estimate that the scattering volumes of SiO_x in S1 and S2 are comparable (radius of SiO_x sphere = 35 nm). The decrease in Raman

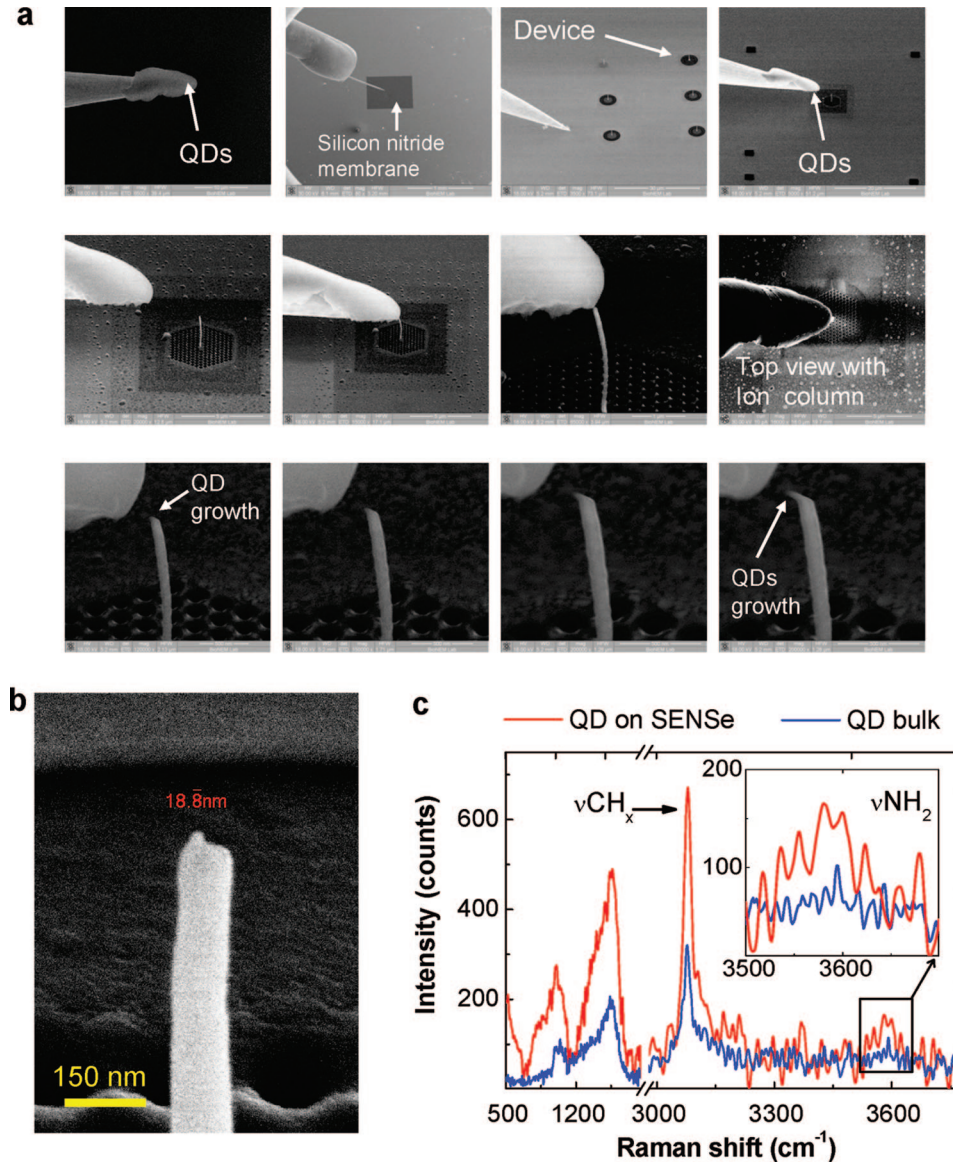

Figure 4. Single quantum dot deposition on the nanoantenna. (a) SEM images arranged in progressive magnification (from top left to bottom right) to show the deposition technique of QDs from the manipulator tip to the nanoantenna. (b) SEM image of a single core−shell ZnS/CdSe QD deposited at the SENSe tip. (c) Raman scattering spectra ($\lambda_{exc} = 514$ nm, $P = 0.18$ mW, $T_{int} = 150$ s) taken from the single QD (red line) as compared to that of a QD bulk sample (blue line). In the inset the asymmetric stretching vibration, aν-NH_2, at 3580 cm^{-1} is reported in the range between 3400 and 3800 cm^{-1}.

scattering intensity is the experimental proof that the SPP intensity probed at S2 is lower with respect to S1, as expected from the calculated field localization. Notice that even if at S3 the scattering volume is about 4 times larger, the Raman intensity is almost at background level (green line). This is expected from the negligible field intensity along the straight portion of the nanoantenna (Supporting Information section 6). This experimental condition is equivalent to having a single isolated particle where no enhancement is present.

Experimental demonstration of the high sensitivity reached by the SENSe device is proved by measuring the Raman signal coming from a single quantum dot (QD). This is accomplished by the use of a nanomanipulator, SEM assisted, whose positioning accuracy in the most critical direction is 0.25 nm (see Supporting Information sections 7 and 8). In Figure 4a SEM images are arranged in a series with progressive magnification (from top left to bottom right) to show the deposition technique of QDs from the manipulator tip to the nanoantenna. The tip of the manipulator has been loaded with QDs by mechanically plowing it in a bulk QD sample (first panel). The deposition of a single QD from the nanomanipulator tip to the nanoantenna tip is not simply due to the mechanical friction but is electrostatically assisted under the SEM beam. We observed that the deposition occurs in two different ways: (a) The nanomanipulator tip and the nanoantenna tip are in close contact and are instantaneously welded by electrostatic forces. By pulling the nanomanipulator tip away from the nanoantenna tip, the QD remains attached to the nanoantenna tip. (b) The nanomanipulator tip and the nanoantenna tip are close but not in contact (200 nm distance). Thanks to the electrical charging of the sample, there is a growing electrical field (estimated field is about

10^6 V/cm) that is strong enough to be able to transfer the QDs from the nanomanipulator tip to the nanoantenna tip (see last four panels in high magnification).

The manipulator allows the deposition of a single QD (QD ITK amino PEG quantum dots ZnS/CdSe Invitrogen, 15−20 nm diameter) on the nanoantenna tip. In Figure 4b, a detailed SEM picture of the deposited single QD is shown. The apparent increase in the radius of curvature of the tip is due to carbon codeposition (see Supporting Information section 4) during the operation time of QD manipulation and deposition. This carbon overlayer is responsible for the C−C vibrational mode at 1591.8 cm^{-1} and of the shoulder at 1353.8 cm^{-1}. In Figure 4c the Raman scattering spectrum of the single QD is compared to a QD bulk assembly of cylindrical shape (1.2 μm diameter and 200 nm thickness, see Supporting Information section 9), as obtained in identical spectroscopic conditions (laser power, substrate material, sample preparation). The Raman intensity peak details from the single QD on the nanoantenna matches the spectroscopic information from the bulk sample, but the Raman spectra from single QD show more clearly the aν-NH_2 asymmetric stretching vibration at 3580 cm^{-1} (Figure 4c, inset). This vibration is in general weak compared to the CH_x one and its presence in the spectrum is due to the tip local field enhancement. A single QD allows an estimate of the number of NH_2 molecules contributing to this Raman vibration. In fact, from the supplier specifications, the QD has an inner core of 2.5 nm radius, on which PEG (poly(ethylene glycol)) molecules are bound with NH_2 terminated groups,[29] thus resulting in an average single QD diameter of about 18 nm. A conservative estimation can be done assuming very high close packing of PEG−NH_2 groups, that is, 1 anchorage per nm^2. With this assumption the total detected number of NH_2 groups is equal to 80 and the Raman scattering signal enhancement is calculated to be about 10^5. When using the anchorage specification given by the QD supplier, the number of amino groups detected is estimated to be 10.

Lastly, a monolayer of BTH is chemisorbed on a gold nanoantenna via covalent bonding of the thiol groups, and its Raman scattering spectrum is shown in Figure 5 (red line). The spectrum is compared with that measured on a bulk BTH sample (Figure 5, blue line); the agreement with the characteristic peaks is evident. The additional peaks on the spectrum are found at 1353.8, 1591.8, and at 2709.5 cm^{-1}, which are attributed to amorphous carbon D-band, G-band, and second-order D-band, respectively. All experiments presented here are designed to check both the plasmonic localization field and the device sensitivity at level of few molecules in SERS conditions. In the first experiments, we experimentally demonstrated, through Raman scattering and controlled deposition at the nanometer level, that the SPP field is strongly localized in a region comparable to the radius of curvature of the nanoantenna tip. This demonstration allows us to infer that also for the BTH monolayer, the intense Raman signals are due to a strong localization and enhancement caused by the efficient generation of SPP in the nanoantenna.

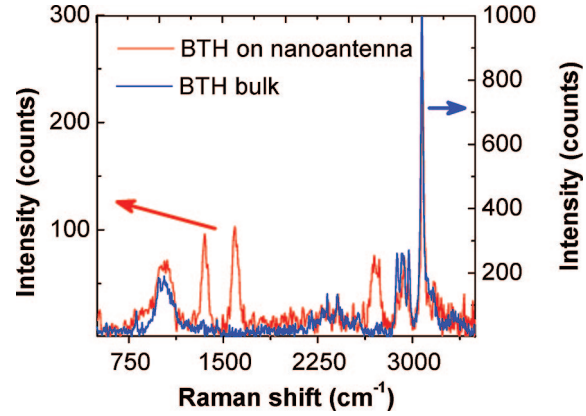

Figure 5. Confocal Raman scattering on BTH. Raman scattering measurements (λ_{exc} = 514 nm, P = 0.18 mW, T_{int}= 100 s) on benzenethiol (BTH) monolayer on the nanoantenna (red line) as compared to the bulk spectrum (blue line).

The field enhancement on the nanoantenna tip is strong enough to allow the detection of a monolayer of molecules deposited on that area. In our standard case, the radius of curvature of the nanoantenna tip is ≈10 nm (lower radius of curvature in Supporting Information section 1). Considering that the surface area of a BTH molecule is about 0.4 nm^2, we estimate that the Raman signal coming from the nanoantenna tip is due to about 200 molecules when close packed. Moreover, the measured enhancement factor of the Raman signal with respect to a BTH bulk sample in a standard Raman configuration is about 3 × 10^6. The calculation is done by considering an underestimated bulk scattering volume with cylindrical shape: base diameter is equal to the 1 μm laser beam diameter and height is equal to the depth of focus estimated in confocal mode (300 nm).

The relevant aspect in the proposed experiments is that we exploit the nanoantenna coupled to a dielectric PC cavity to convert the intrinsically evanescent SPP field into a propagating e.m. signal to be detected through Raman scattering in the far field. In this way, the device avoids experimental difficulties associated to the use of a near-field configuration. Moreover, the design and label-free scheme allow for realistic and reproducible detection of few molecules with subwavelength spatial confinement in far-field configuration. The high sensitivity and the high signal-to-noise ratio found in the experimental Raman spectra of the present work open bright perspectives for application to single molecule detection. Our device can straightforwardly be combined with scanning probe microscopes such as AFM (Supporting Information section 10) with the possibility to match the topographical landscape with the force and chemical spectroscopic mapping at the same nanometer length scale.

Acknowledgment. In memory of Professor Salvatore Venuta. Thanks to his help, effort, and encouragement this activity became a reality. This work is supported by the Italian Ministry of University and Research under the MIURPRIN2005039992 project and FIRB Contract RBAP06L4S5, as well as by the CARIPLO Foundation.

Supporting Information Available: Information regarding the plasmonic nanoantenna, design and optical response of the overall device, the experimental Raman setup, SiO_x deposition on the nanoantenna, microanalysis of the nanoantenna, Raman scattering measurements on SiO_x nanoparticles deposited on a nanoantenna, the nanomanipulator, Raman scattering measurements on QD samples, Raman scattering measurements on a single QD nanoantenna, on and off resonance, and FDTD simulation, and SENSe on the atomic force microscope cantilever. This material is available free of charge via the Internet at http://pubs.acs.org.

References

(1) Drachev, V. P.; Thoreson, M. D.; Khaliullin, E. N.; Davisson, V. J.; Shalaev, V. M. *J. Phys. Chem. B* **2004**, *108*, 1846–1852.
(2) Hell, S. W. *Science* **2007**, *316*, 1153–1158.
(3) Taminiau, T. H.; Moerland, R. J.; Segerink, F. B.; Kuipers, L.; van Hulst, N. F. *Nano Lett.* **2007**, *7*, 28–33.
(4) Xu, H.; Bjerneld, E. J.; Kall, M.; Borjesson, L. *Phys. Rev. Lett.* **1999**, *83*, 4357–4360.
(5) Nie, S.; Emory, S. R. *Science* **1997**, *275*, 1102–1106.
(6) Kneipp, K.; Wang, Y.; Kneipp, H.; Perelman, L. T.; Itzkan, I.; Dasari, R. R.; Feld, M. S. *Phys. Rev. Lett.* **1997**, *78*, 1667–1670.
(7) Hecht, B.; Bielefeldt, H.; Novotny, L.; Inouye, Y.; Pohl, D. W. *Phys. Rev. Lett.* **1996**, *77*, 1889–1892.
(8) Pendry, J. *Science* **1999**, *235*, 1687–1688.
(9) Barnes, W. L.; Dereux, A.; Ebbesen, T. W. *Nature* **2003**, *424*, 824–830.
(10) Bozhevolnyi, S. I.; Volkov, V. S.; Devaux, E.; Laluet, J. Y.; Ebbesen, T. W. *Nature* **2006**, *440*, 508–511.
(11) Malynych, S.; Robuck, H.; Chumanov, G. *Nano Lett.* **2001**, *1*, 647–649.
(12) Yu, A. A.; Savas, T.; Cabrini, S.; Di Fabrizio, E.; Smith, H. I.; Stellacci, F. *J. Am. Chem. Soc.* **2005**, *127*, 16775.
(13) Hering, K.; Cialla, D.; Ackermann, K.; Dorfer, T.; Moller, R.; Schneidewind, H.; Mattheis, R.; Fritzsche, W.; Rosch; P.; Popp, J. *Anal. Bioanal. Chem.* **2008**, *390*, 113 and references therein.
(14) Hartschuh, A.; Pedrosa, H. N.; Novotny, L.; Krauss, T. D. *Science* **2003**, *301*, 1354.
(15) Hartschuh, A.; Sanchez, E. J.; Xie, X. S.; Novotny, L. *Phys. Rev. Lett.* **2003**, *90*, 095503-1-4.
(16) Verma, P.; Yamada, K.; Watanabe, H.; Inouye, Y.; Kawata, S. *Phys. Rev. B* **2006**, *73*, 045416.
(17) Zenobi, R. *Anal. Bioanal. Chem.* **2008**, *390*, 215 and references therein.
(18) Ditlbacher, H.; Hohenau, A.; Wagner, D.; Kreibig, U.; Rogers, M.; Hofer, F.; Aussenegg, F. R.; Krenn, J. R. *Phys. Rev. Lett.* **2005**, *95*, 257403.
(19) Xu, H.; Aizpurua, J.; Kall, M.; Apello, P. *Phys. Rev. E* **2000**, *62*, 4318–4324.
(20) Gerace, D.; Galli, M.; Bajoni, D.; Guizzetti, G.; Andreani, L. C.; Riboli, F.; Melchiorri, M.; Daldosso, N.; Pavesi, L.; Pucker, G.; Cabrini, S.; Businaro, L.; Di Fabrizio, E. *Appl. Phys. Lett.* **2005**, *87*, 211116.
(21) Stockman, M. I. *Phys. Rev. Lett.* **2004**, *93*, 137404.
(22) Ropers, C.; Neacsu, C. C.; Elsaesser, T.; Albrecht, M.; Raschke, M. B.; Lienau, C. *Nano Lett.* **2007**, *7*, 2784.
(23) Verhagen, E.; Kuipers, L.; Polman, A. *Nano Lett.* **2007**, *7*, 334–337.
(24) Nanofabrication Center, University of Minnesota http://www.nfc.umn.edu, cibuzar@umn.edu.
(25) Akahane, Y.; Asano, T.; Song, B.-S.; Noda, S. *Nature* **2003**, *425*, 944–947.
(26) Andreani, L. C.; Gerace, D. *Phys. Rev. B* **2006**, *73*, 235114.
(27) Taflove, A. *Computational Electrodynamics: The Finite-Difference Time-Domain Method*, 3rd ed.; Artech House: Boston, MA, 2005.
(28) Roden, J. A.; Gedney, S. D. *Microwave Opt. Technol. Lett.* **2000**, *27*, 334–339.
(29) www.invitrogen.com.

NL801112E